

A Spline-based Partial Element Equivalent Circuit Method for Electrostatics

Riccardo Torchio, Maximilian Nolte, Sebastian Schöps, Albert E. Ruehli[†]

September 29, 2022

Abstract

This contribution investigates the connection between Iso-geometric Analysis (IgA) and the Partial Element Equivalent Circuit (PEEC) method for electrostatic problems. We demonstrate that using the spline-based geometry concepts from IgA allows for extracting circuit elements without a meshing step. Moreover, the proposed IgA-PEEC method converges for complex geometries up to three times faster than the conventional PEEC approach and, in turn, it requires a significantly lower number of degrees of freedom to solve a problem with comparable accuracy. The resulting method is closely related to the isogeometric boundary element method. However, it uses lowest-order basis functions to allow for straightforward physical and circuit interpretations. The findings are validated by an analytical example with complex geometry, i.e., significant curvature, and by a realistic model of a surge arrester.

Keywords: electrostatics, partial element equivalent circuit, isogeometric analysis, splines

1 Introduction

Numerical simulation tools based on discretizations of Maxwell's equations are established in academia and industry. They support engineers during the design and analysis of products like electric surge arresters or high voltage devices [1, 2]. They are particularly popular when designing complex geometries that cannot be analyzed in closed-form or by simple electric circuit models.

Most such numerical methods are based on surface or volume meshes that approximate the geometry with low order elements, e.g., triangles. This comes with two drawbacks: First, there is a geometry error that is only acceptable if it does not impede the overall convergence of the method. Secondly, the meshing step may be time consuming and error prone. Its contribution to the overall workflow can be

^{*}This work is supported by the Graduate School CE within the Centre for Computational Engineering at TU Darmstadt, by the German Research Foundation via the project 443179833 and the DAAD in the framework of Short-Term Grants (57588366). The authors thank Felix Wolf, Jürgen Dölz, and Stefan Kurz for the fruitful discussions on the topic. (*Corresponding author:* Riccardo Torchio). Riccardo Torchio was with the Department of Industrial Engineering, Università degli Studi di Padova. Maximilian Nolte and Sebastian Schöps were with the Computational Electromagnetics group, Technische Universität at Darmstadt. Albert E. Ruehli was with the EMC Laboratory of Missouri University of Science & Technology.

[†]Manuscript received April 19, 2021; revised August 16, 2021.

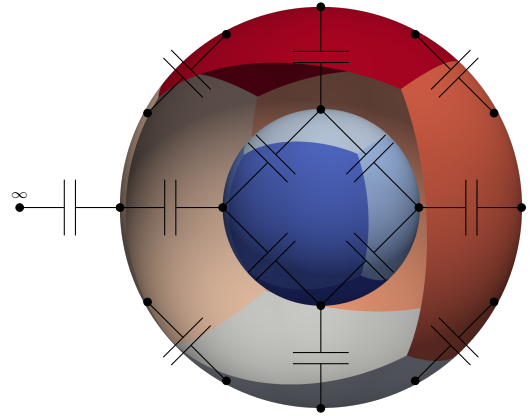


Figure 1: Interpretation of the coefficients $C_{k,l}$ as capacities, the remaining capacities are being omitted for the purpose of visual clarity.

significant, Sandia labs have analyzed that about 75% of the simulation time is related to modeling, parameterization, mesh generation and pre- and post-processing [3]. In contrast, Isogeometric Analysis (IgA), [4], makes use of the exact representation of a device's geometry in the language of Computer Aided Design (CAD) tools. Most common CAD tools use boundary representations (B-rep) of objects based on patches of Non Uniform Rational B-Splines (NURBS). NURBS are popular since they can describe conic sections exactly, enable local smoothness control, and allow defining curves and surfaces intuitively [5].

We propose to formulate the electrostatic problem in terms of integral equations based on the same NURBS geometry descriptions used in IgA. Consequently, there is no geometrical approximation error and no need of a separate meshing step. We follow the well-known Partial Element Equivalent Circuit (PEEC) scheme [6]. It allows for an automatic representation of the problem by means of an equivalent electric circuit, see Fig. 1. Eventually, the circuit can be solved in a SPICE-like solver, possibly combined with other circuits that represent other devices and/or parts of the system. For example, nonlinear models that are popular to describe varistor-based stress control of high-voltage surge arresters [7], can be easily included. Being in the isogeometric setting, we use the term patch instead of the term cell commonly used in PEEC methods. The usage of the two terms is equivalent.

The original PEEC method [6, 8] is based on subdividing the computational domain in simple structures, e.g., regular hexahedra or rectangular patches, that allow exact and fast quadrature of the involved integrals. During the years,

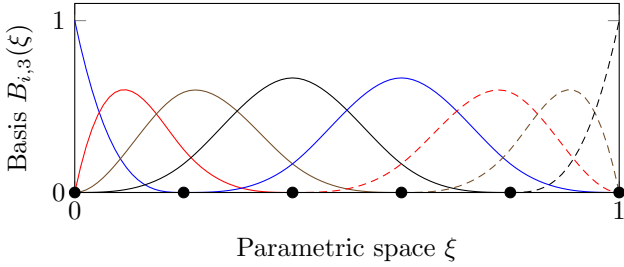


Figure 2: B-Splines basis functions of degree 3.

the PEEC method has been extended to the case of more general mesh elements, such as non-orthogonal hexahedral elements [9], tetrahedral elements [10], etc. However, in the literature only linear (non-curved) elements and lowest order basis functions have been used in the context of PEEC. Therefore, geometrical approximation errors are unavoidable when dealing with complex freeform geometries, e.g., devices with curvatures [11].

Our implementation is based on an existing isogeometric boundary element library [12, 13]. It is shown that using this framework with lowest-order basis functions for the expansion of the solution, i.e., one degree of freedom (electric charge) per patch and high-order rational basis functions for the geometry, a PEEC method is obtained that fulfills all promises mentioned above. In particular, it is demonstrated using the example of a spherical capacitor, that the convergence rate of this new method is optimal while the rate deteriorates when using conventional PEEC implementations. This is explained by the fact that the so-called Aubin-Nitsche trick, e.g., [14], is not applicable due to the geometric modelling error.

Consequently, the proposed combination of technologies contributes to bridging the gap between CAD and circuit simulation. The rest of the paper is organized as follows. In Section 2, the fundamentals of CAD and NURBS is revisited. Moreover, the specific choice of the shape functions used to apply the PEEC discretization scheme is discussed. In Section 3 the PEEC formulation for the electrostatic case is briefly described, as well as the use of patch-wise defined B-splines to discretize the unknowns. Section 3.2 revise the PEEC stamping techniques for the specific case of electrostatic problems, therefore it is shown how a *net-list* can be automatically constructed from the matrix coefficients generated by the IgA-PEEC method. Finally, in Section 4 the findings are validated by considering an analytical example with complex geometry, i.e., significant curvature, and a realistic model of a surge arrester.

2 Splines and Geometry

We assume that the CAD geometry is represented by the union of N_Γ surface patches given in terms of NURBS. Each patch is constructed from two (weighted) b-spline curves. The basis $\{B_{i,p}\}_{i=1}^{N_1}$ of a one-dimensional B-spline space \mathbb{S}_α^p of degree p and regularity α is determined by the knot vector $\Xi = (\xi, \xi', \dots, \xi_n) \in [0, 1]^n$, $\xi \leq \xi' \leq \dots \leq \xi_n$.

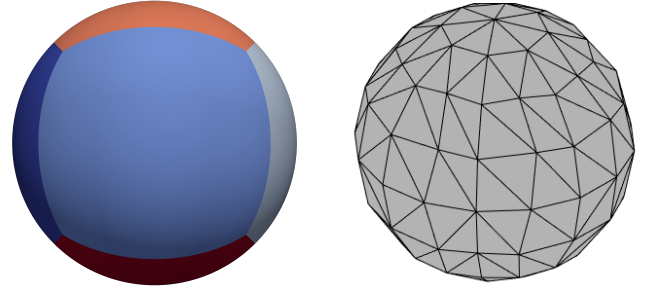


Figure 3: Exact description of a sphere by $N_\Gamma = 6$ NURBS patches (left) and approximation of a sphere by 208 triangles (right).

The basis is then given by the Cox-de Boor algorithm

$$B_{i,0}(\xi) = \begin{cases} 1 & \text{if } \xi_i \leq \xi < \xi_{i+1} \\ 0 & \text{otherwise} \end{cases} \quad (1)$$

and for $p > 0$

$$B_{i,p}(\xi) = \frac{\xi - \xi_i}{\xi_{i+p} - \xi_i} B_{i,p-1}(\xi) + \frac{\xi_{i+p+1} - \xi}{\xi_{i+p+1} - \xi_{i+1}} B_{i+1,p-1}(\xi).$$

Fig. 2 shows a visualization of the basis functions in of degree $p = 3$. A corresponding NURBS curve is obtained by

$$\gamma(\xi) = \sum_{i=1}^k \frac{B_{i,p}(\xi) w_i \mathbf{p}_i}{\sum_{q=1}^k B_{q,p}(\xi) w_q} \quad (2)$$

where k is the number of control points \mathbf{p}_i and w_i are the weights. Finally, the n -th patch can be described as a NURBS mapping from the reference space $[0, 1] \times [0, 1]$ to the three-dimensional physical space as

$$\Gamma_n(\xi, \xi') = \sum_{i=1}^k \sum_{j=1}^l \frac{B_{i,n}(\xi) B_{j,m}(\xi') w_{i,j} \mathbf{p}_{i,j}}{\sum_{q=1}^k \sum_{r=1}^l B_{q,n}(\xi) B_{r,m}(\xi') w_{q,r}}. \quad (3)$$

Consequently, each distinct conductive domain in the problem is exactly described by the union of a connected set of such patches. Since we are focusing on electrostatic problems, the connected patches making up a domain will be equipotential. We also refer to them as electrodes.

In contrast to many other approaches, only a few patches are sufficient to describe even complex objects, e.g., $N_\Gamma = 6$ NURBS surfaces determine exactly a sphere, see Fig. 3 (left). Now, when computing integrals on such a surface, e.g., the area $\int_\Gamma d\Gamma'$, then one can use patch-wise Gaussian quadrature on the reference domain using push-forwards [15]. The convergence is only determined by the order of the quadrature rule. In contrast, each element of a low-order surface mesh, e.g., shown in Fig. 3 (right), can be exactly evaluated but is limited to low-order convergence. Please note that the quadrature in both cases can be easily parallelized.

3 Electrostatic PEEC Method

The electrostatic PEEC formulation [8, eq: (3.52)] starts from the well-known electrostatic field equations:

$$\nabla \cdot \mathbf{D} = \rho, \quad (4)$$

$$\mathbf{E} = -\nabla\varphi, \quad (5)$$

where φ is the scalar electric potential, ρ is the charge density, \mathbf{E} is the electric field, and \mathbf{D} is the electric displacement field.

For the case where conductive media and free space are considered, \mathbf{D} and \mathbf{E} are linked by the following constitutive equation

$$\mathbf{D} = \varepsilon_0 \mathbf{E}, \quad (6)$$

where ε_0 is the vacuum permittivity.

Substituting (6) into (4) and using (5) the following Poisson equation is obtained

$$\nabla \cdot \mathbf{E} = -\nabla^2 \varphi = \frac{\rho}{\varepsilon_0}. \quad (7)$$

The Poisson equation (7) can then be reformulated in terms of Green function $g(\mathbf{r}, \mathbf{r}')$, i.e., the solution of

$$\nabla^2 g(\mathbf{r}, \mathbf{r}') = -\delta(\mathbf{r} - \mathbf{r}'), \quad (8)$$

where \mathbf{r} is the field point, \mathbf{r}' is the integration point, δ is the Dirac delta function, and

$$g(\mathbf{r}, \mathbf{r}') = \frac{1}{4\pi\|\mathbf{r} - \mathbf{r}'\|}. \quad (9)$$

By using (8) and (9) into (7), the integral solution of the Poisson equation is obtained

$$\varphi(\mathbf{r}) = \frac{1}{4\pi\varepsilon_0} \int_{\Gamma} \frac{\rho(\mathbf{r}')}{\|\mathbf{r} - \mathbf{r}'\|} d\Gamma', \quad (10)$$

where Γ is the boundary of the conductive domains in terms of NURBS.

For the representation of the fields we may use patch-wise defined B-splines from the space

$$\mathbb{S}_{\alpha}^p(\Gamma) = \{f: f|_{\Gamma_k} \in \mathbb{S}_{\alpha}^p(\Gamma_k), 1 \leq k \leq N_{\Gamma}\}, \quad (11)$$

with $\mathbb{S}_{\alpha}^p(\Gamma_k) = \{f: (f \circ \Gamma_k) \in \mathbb{S}_{\alpha}^p \times \mathbb{S}_{\alpha}^p\}$, see [16]. The goal is to find a discrete solution $\rho_h \in \mathbb{S}_{\alpha}^p(\Gamma)$, which yields the applied potential φ when inserted into (10) and evaluated on the electrodes. For this we choose a basis $\{w_i\}_{1 \leq i \leq n}$, with $n = \dim(\mathbb{S}_{\alpha}^p(\Gamma))$ which fulfills $\text{span}\{w_1, \dots, w_n\} = \mathbb{S}_{\alpha}^p(\Gamma)$. In the particular case of $p = 0$ and without mesh refinement, i.e., $i = k$, we choose w_k such that $\hat{w}_k = (w_k \circ \Gamma_k) = 1/|\Gamma_k|$ holds, where $|\Gamma_k|$ denotes the area of the corresponding patch Γ_k . Utilizing the Galerkin discretization $\rho_h = \sum_{i=1}^n q_i w_i$ yields the discrete variational problem: find $\rho_h \in \mathbb{S}_{\alpha}^p(\Gamma)$ such that

$$\frac{1}{4\pi\varepsilon_0} \int_{\Gamma} w_j(\mathbf{r}) \int_{\Gamma} \frac{\rho_h(\mathbf{r}')}{\|\mathbf{r} - \mathbf{r}'\|} d\Gamma' d\Gamma = \int_{\Gamma} \varphi(\mathbf{r}) w_j(\mathbf{r}) d\Gamma, \quad (12)$$

for all test functions $w_j \in \mathbb{S}_{\alpha}^p(\Gamma)$.

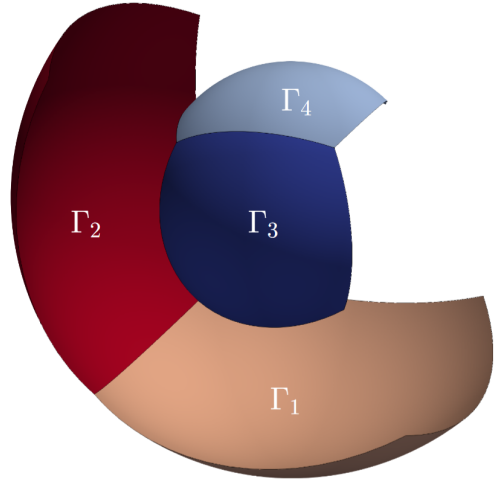


Figure 4: NURBS patches for a simple case with two domains. Each domain is discretized by two patches.

3.1 Quadrature and Solution of the Linear System

For the assembly of the Galerkin system matrix (12), we need to deal with singular integrals and use the Duffy trick [17]. Additionally, one has to increase the quadrature degree logarithmically with the distance between the evaluated elements [14]. Furthermore, in the utilized implementation Bembel [13], the assembly is performed in parallel.

After numerical quadrature, the problem (12) corresponds to a linear equation system

$$\mathbf{P}\mathbf{q} = \boldsymbol{\phi}, \quad (13)$$

where \mathbf{q} is the coefficient vector describing the charge distribution ρ_h , \mathbf{P} is the potential IgA-PEEC matrix and $\boldsymbol{\phi}$ contains the potentials. The general ij th coefficient of such matrix is given by

$$P_{ij} = \frac{1}{4\pi\varepsilon_0} \int_{\Gamma} w_j(\mathbf{r}) \int_{\Gamma} \frac{w_i(\mathbf{r}')}{\|\mathbf{r} - \mathbf{r}'\|} d\Gamma' d\Gamma. \quad (14)$$

In contrast to (high-order) isogeometric boundary elements methods, we chose element-wise constant basis functions ($p = 0$). In the simplest case, i.e., without mesh refinement, the entries of \mathbf{q} can be interpreted as patch-wise charges. Consequently, $\mathbf{C}_M = \mathbf{P}^{-1}$ can be interpreted as the (full) Maxwell capacitance matrix from which the short circuit capacitance matrix \mathbf{C} can be easily obtained as shown in [8], where C_{kl} , with $k \neq l$, is a capacitance connecting the patches Γ_k and Γ_l , see Fig. 1. Finding \mathbf{C} requires the inversion of matrix \mathbf{P} , that can be computationally expensive. Moreover, as discussed in [8], some meshing related accuracy problems may occur when matrix \mathbf{C} want to be obtained from \mathbf{P} . For this reason and in the same fashion of the standard PEEC method, with the aim of automatically construct an equivalent electric circuit of (13) that can be loaded and solved into a SPICE-like solver, the current source-based stamping technique described in the next section can be adopted instead.

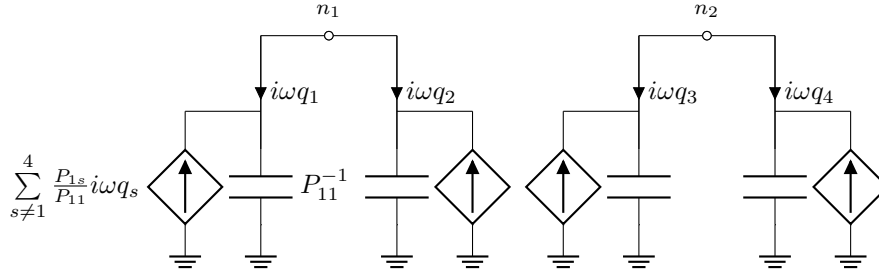


Figure 5: Equivalent circuit obtained by exploiting the electrostatic PEEC scheme related to the case represented in Fig. 4.

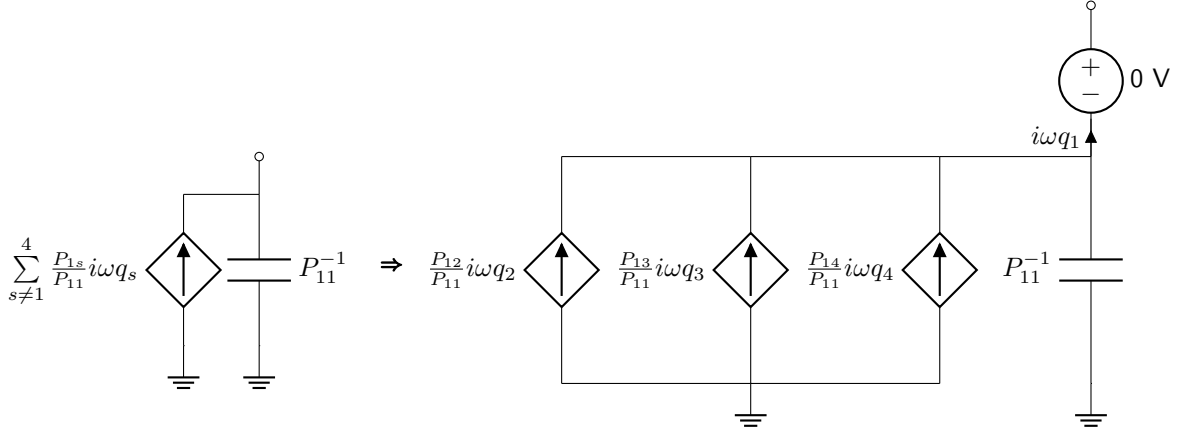


Figure 6: Representation of the current controlled current sources.

3.2 Stamping Technique

The electrostatic IgA-PEEC problem can be solved with any standard technique for solving linear systems (e.g., LU decomposition). Alternatively, by exploiting the circuit interpretation provided by the PEEC scheme, an equivalent circuit and a *net-list* can be constructed and the problem can be imported into a SPICE-like solver where it can be solved and possibly coupled with other circuits representing other devices or parts of the system. In this section, the stamping technique which allows to automatically construct an equivalent *net-list* of the problem is changed for the specific case of electrostatic problems.

In some applications, it can be convenient to represent the fully coupled electrostatic problem (13) in terms of an equivalent circuit. Thus, a *net-list* which represents the electrostatics problem can be generated. Then, such *net-list* can be loaded into a SPICE-like solver where it can be coupled with other circuits. This can be particularly useful when one wants to couple the *net-list* representing the electrostatic problem with complex circuit components that are described by dedicated networks provided by the SPICE-like solver but not accessible to the user (e.g., varistor-based stress control of high-voltage surge arresters). In the following, it is described how to automatically construct a *net-list* equivalent to (13).

For electrostatic problems, the standard PEEC primary circuit cell [18] can be simplified with respect to the one related to full-Maxwell problems. For the sake of clarity, the very simple problem showed in Fig. 4 can be considered, where two thin and curved conductive domains are shown. Each one of the two domains is discretized by two patches.

Although very simple, this model allow us to discuss how to automatically construct the *net-list* for general models. It is worth noting that, although the formulation described in this paper has been developed for electrostatic problems only, once the *net-list* equivalent to (13) is constructed and loaded into the SPICE-like solver, the *net-list* can be coupled with other circuits and also frequency or time domain simulations can be performed. Thus, for the sake of generality, in this section the discussion is carried on by considering a frequency domain problem since the extension is straightforward. Fig. 5 shows the equivalent circuit of the model in Fig. 4. All the patches that make up a distinct domain are equipotential, therefore the equivalent circuit has a number of nodes equal to the number of separate domains plus one node for the ground which is at an infinite distance from the devices. The number of patches is indicated with N , and in this case $N = 4$.

Thus, the electric potential value of patch Γ_1 and patch Γ_2 in Fig. 4 is given by the potential of node 1 in Fig. 5. Analogously, the electric potential value of patch Γ_3 and patch Γ_4 in Fig. 4 is given by the potential of node 2 in Fig. 5.

The connections between the patches (circuit nodes) and the ground node are instead modelled with equivalent capacitances and Current Controlled Current Sources (CCCSs). The equivalent capacitances represent the electrostatic interaction between a single patch and the infinity and they are given by

$$C_{ii} = \frac{1}{P_{ii}}. \quad (15)$$

Instead, the CCCSs represent the electrostatic interactions

Algorithm 1 Automatic *net-list* generation.

Input: Matrix \mathbf{P} and domain tag for each patch

Generate void `netlist.cir` file {0}

Stamping capacitances and zero VSs in series {1}

for $i=1, \dots, N$ **do**

Find domain tag of the i -th patch, i.e.,

$d = \text{domain_tag}(i)$

In a new line of `netlist.cir`, print:

`C_#i 0 #i P_{ii}^{-1} ;`

In a new line of `netlist.cir`, print:

`V_#i #i #d 0;`

end for

Stamping CCCSs {2}

for $i=1, \dots, N$ **do**

for $j=1, \dots, N$ **do**

In a new line of `netlist.cir`, print:

`F_#i#j 0 #i V_#j P_{ji}/P_{ii} ;`

end for

end for

If required, add other circuit components {3}

Output: *net-list* printed in `netlist.cir` file

between different patches. It is worth noting that each CCCS represented in Fig. 5 should be modelled by $N - 1$ CCCSs representing the mutual interaction between two patches (see Fig. 6) with gain X given by the ratio between the mutual potential coefficient of the two patches and the self potential coefficients of the patches connected to the CCCS, i.e.,

$$X_{ij} = \frac{P_{ij}}{P_{ii}}. \quad (16)$$

It is worth noting that each CCCS component at the right part of Fig. 6 is controlled by the current $i\omega q_i$. At the circuit level, this current can be obtained by summing up the contributions of the current flowing through the i th capacitance and all currents flowing in the CCCSs connected in parallel to the capacitance. Thus, as described in [19], to make this current available in the *net-list*, a Voltage Source (VS) imposing a zero voltage must be added in series to each capacitance. Thus, by taking Fig. 5 as example, 4 VSs imposing zero voltage are added to the *net-list* and they are connected to the upper terminal of each capacitance and to nodes n_1 and n_2 as shown in Fig. 6.

Finally, once the PEEC potential matrix is constructed it is possible to automatically generate the equivalent *net-list* by using Algorithm 1, where all the required components described above (i.e., capacitances, CCCSs, and zero voltage VSs) are stamped.

From the discussion above, it can be inferred that the generated *net-list* consist of a large number of components since all the mutual couplings between the patches require a circuit component. As discussed in [20], this can become an issue when a large number of unknowns is required since standard SPICE-like solvers may be inefficient when

large systems of equations with dense matrix blocks are generated. However, it is worth noting that the high-order curved geometry description allows for keeping small the number of required patches, thus mitigating such issue.

3.3 Convergence

For sufficiently smooth geometries Γ and solutions φ of (7) the expected convergence order of the approximation ρ_h is $\mathcal{O}(h^{3/2+p})$. This is a consequence of the convergence theory for boundary element methods [14, Cor. 4.1.34]. The error of the potential evaluated in (10) by inserting ρ_h converges even faster, i.e. with $\mathcal{O}(h^{3+2p})$ due to the Aubin-Nitsche trick [14, Thm. 4.2.14]. This trick holds more generally for any linear functional of the approximation ρ_h that can be evaluated with sufficient accuracy. Since we obtain the capacities, see (14), in the isogeometric approach by surface integration based on the exact geometry, we also profit here from the increased convergence rate.

4 Numerical Results

In this section, simulation results obtained from numerical experiments are shown. Two test cases are considered. The first is an academic example consisting of a spherical capacitor, i.e., two concentric spheres. While being simple, this test case allow us to show the benefits of the proposed spline-based PEEC approach due to its strong curvature. Moreover, this problem has a closed-form solution and therefore we can test and compare the accuracy of the numerical methods.

The second test case instead consists on the realistic model of a surge arrester. In this model, thanks to the circuit interpretation provided by the PEEC scheme, the surge arrester model is excited by using a lumped voltage source.

The proposed PEEC method has been implemented within the Bembel, The fast isogeometric boundary element C++ library [13]. The implementation provides an interface to the Eigen template library for linear algebra operations [21]. Furthermore, the matrix assembly is openMP parallelized [22]. For comparison we also use the Matlab implementation of PEEC introduced in [10] based on low-order surface mesh (i.e., triangular elements) and zero-order shape functions. All code is executed on a cluster with Intel® Xeon® Platinum 8160 CPU @ 2.10GHz.

4.1 Academic Example: Two Concentric Spheres

The method has been applied to the electrostatic configuration of two concentric perfect electric conducting spherical shells of radii $r_{\text{in}} = 0.1$ m and $r_{\text{out}} = 0.2$ m. The model shown in Fig. 1 consists of 12 NURBS patches. Without further refinement, this leads to 78 partial capacitances with total capacitance of $C = 21.5$ pF. The reference value is the closed-form solution [23]

$$C_{\text{ana}} = \frac{4\pi\epsilon_0}{(1/r_{\text{in}} - 1/r_{\text{out}})} \approx 22.25 \text{ pF}.$$

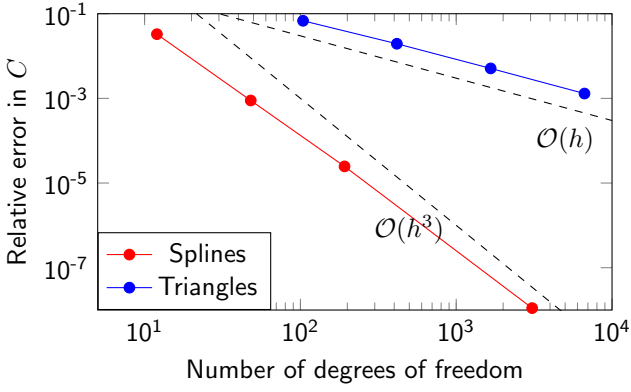


Figure 7: Convergence analysis of the relative error of the numerically computed capacity plotted against the utilized degrees of freedom. The new method is denoted by ‘Splines’ and a conventional reference implementation by ‘Triangles’.

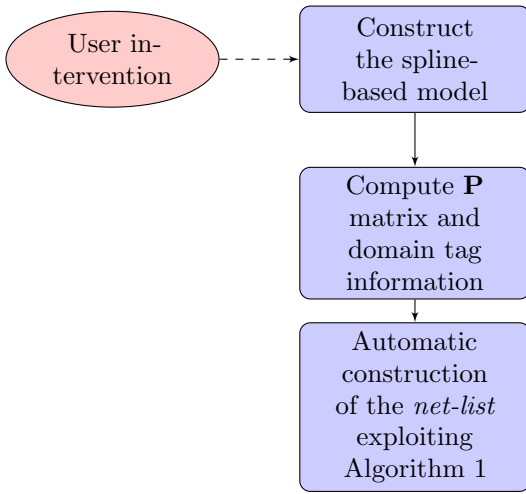


Figure 8: Work-flow for the automatic *net-list* generation.

The slopes for the isogeometric method shown in Fig. 7 obtained by mesh refinement meet the expected optimal convergence order of $\mathcal{O}(h^3)$ for lowest-order basis functions, see Section 3.3. On the other hand, Fig. 7 also shows the results obtained from the standard PEEC method based on low-order surface mesh (i.e., triangular elements) and zero-order shape functions. Here, the convergence is limited to first order since we do not evaluate the surface integral with sufficient accuracy and the Aubin-Nitsche trick is not applicable. This is well-known in the context of boundary element methods, see for example [14, Tbl. 8.2] for an overview of the necessary orders of curvature approximations. The two curves in Fig. 7 confirm the theoretical prediction that the convergence order of the proposed spline based PEEC method is much higher than (non-curved) triangle-based PEEC approaches.

The results above and in Fig. 7 were obtained by solving (13) with the LU decomposition implemented in Eigen [21]. However, for the sake of completeness, the automatic construction of the *net-list* as discussed in Section 3.2 and schematically reported in Fig. 8 is also performed. The generated *net-list* is loaded into the SPICE-Solver LTspice and solved by executing the circuit simulator. The

```

* my netlist
C 1 0 1 5.0964e-11; capacitance of patch #1 w.r.t. infinity
C 2 0 2 5.0964e-11; capacitance of patch #2 w.r.t. infinity
C 3 0 3 5.0964e-11; capacitance of patch #3 w.r.t. infinity
C 4 0 4 5.0964e-11; capacitance of patch #4 w.r.t. infinity
C 5 0 5 5.0964e-11; capacitance of patch #5 w.r.t. infinity
C 6 0 6 5.0964e-11; capacitance of patch #6 w.r.t. infinity
C 7 0 7 1.0193e-10; capacitance of patch #7 w.r.t. infinity
C 8 0 8 1.0193e-10; capacitance of patch #8 w.r.t. infinity
C 9 0 9 1.0193e-10; capacitance of patch #9 w.r.t. infinity
C 10 0 10 1.0193e-10; capacitance of patch #10 w.r.t. infinity
C 11 0 11 1.0193e-10; capacitance of patch #11 w.r.t. infinity
C 12 0 12 1.0193e-10; capacitance of patch #12 w.r.t. infinity
V 1 13 1 0; 0-voltage source to measure the displacement current in patch #1
V 2 13 2 0; 0-voltage source to measure the displacement current in patch #2
V 3 13 3 0; 0-voltage source to measure the displacement current in patch #3
V 4 13 4 0; 0-voltage source to measure the displacement current in patch #4
V 5 13 5 0; 0-voltage source to measure the displacement current in patch #5
V 6 13 6 0; 0-voltage source to measure the displacement current in patch #6
V 7 14 7 0; 0-voltage source to measure the displacement current in patch #7
V 8 14 8 0; 0-voltage source to measure the displacement current in patch #8
V 9 14 9 0; 0-voltage source to measure the displacement current in patch #9
V 10 14 10 0; 0-voltage source to measure the displacement current in patch #10
V 11 14 11 0; 0-voltage source to measure the displacement current in patch #11
V 12 14 12 0; 0-voltage source to measure the displacement current in patch #12
F 1 2 0 1 V 2 0.39693; current control current source #1,2
F 1 3 0 1 V 3 0.39693; current control current source #1,3
F 1 4 0 1 V 4 0.39693; current control current source #1,4
F 1 5 0 1 V 5 0.39693; current control current source #1,5
F 1 6 0 1 V 6 0.26034; current control current source #1,6
F 1 7 0 1 V 7 0.34106; current control current source #1,7
F 1 8 0 1 V 8 0.22821; current control current source #1,8
F 1 9 0 1 V 9 0.22821; current control current source #1,9
F 1 10 0 1 V 10 0.22821; current control current source #1,10
F 1 11 0 1 V 11 0.22821; current control current source #1,11
F 1 12 0 1 V 12 0.17144; current control current source #1,12
F 2 1 0 2 V 1 0.39693; current control current source #2,1
F 2 3 0 2 V 3 0.39693; current control current source #2,3
F 2 4 0 2 V 4 0.26034; current control current source #2,4
F 2 5 0 2 V 5 0.39693; current control current source #2,5
  
```

Figure 9: First 41 lines of the generated *netlist.cir* file for the concentric sphere shells test case.

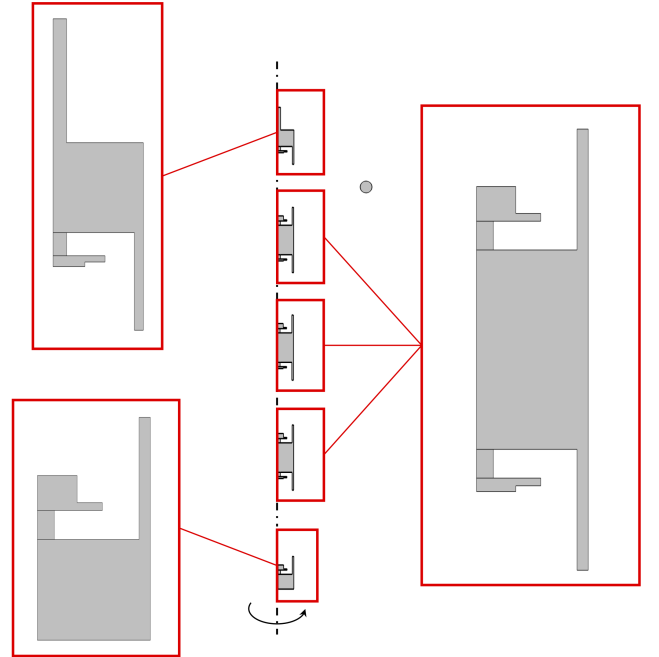


Figure 10: Axisymmetric representation of the surge arrester model derived from [25], with grading ring from [26, Tbl. 4.1], not to scale.

obtained results are, as expected, identical to the one obtained from LU decomposition up to machine precision. A part of the generated *netlist.cir* file is shown in Fig. 9 for illustration; the code is available in [24].

4.2 Surge Arrester

In this section, the model of a realistic surge arrester is considered. The geometry and the dimensions of the model are shown in Fig. 10 and they are derived from [25]. The

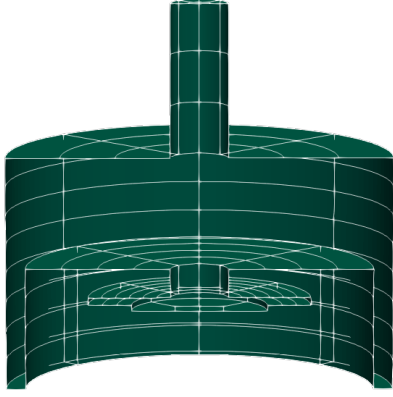


Figure 11: Exemplary representation of top domain of the surge arrester in the NURBS parametrization.

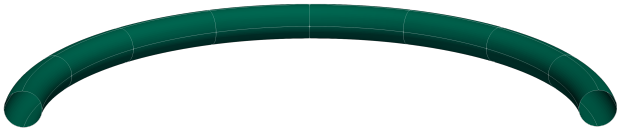


Figure 12: Exemplary representation of the conductive ring of the surge arrester in the NURBS parametrization.

model consists on five metallic domains placed one over the other plus a conductive ring. A voltage source applying 1 V is placed between the top and the bottom metallic domain. Moreover, the ring and the top metallic domain are connected with a circuit short thus they are at the same potential.

Using the spline-based PEEC method, the model consists of 1912 patches, resulting in 30592 elements with twofold uniform refinement. Fig. 12 and Fig. 11 show a detail of the conductive ring and top domain spline based PEEC model, respectively.

By using the standard PEEC method with triangular elements, the model consists on 30113 degrees of freedoms. The capacitance value obtained by using a classical Finite Element Method approach implemented in the commercial software COMSOL® is considered as external reference. The (axisymmetric) FEM model consists of 883297 degrees of freedoms and cubic elements. The value of equivalent capacitance of the structure obtained from the (axisymmetric) FEM model and the spline and triangular based PEEC methods are in very good agreement, i.e., 9.2935 pF, 9.2942 pF, and 9.2715 pF, respectively.

Finally, Fig. 13 and Fig. 14 show the surface charge density distribution on the structure obtained from from the spline and triangular based PEEC methods, respectively. As can be seen, thanks to the perfect representation of the curved geometry by means of splines, the charge density distribution obtained from the spline based PEEC method is smoother than the one obtained from the triangular based PEEC approach.

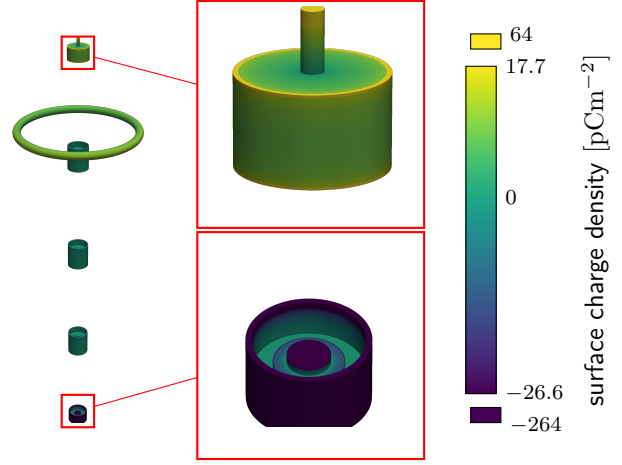


Figure 13: Visualization of the computed surface charge density distribution obtained from the spline-based PEEC method.

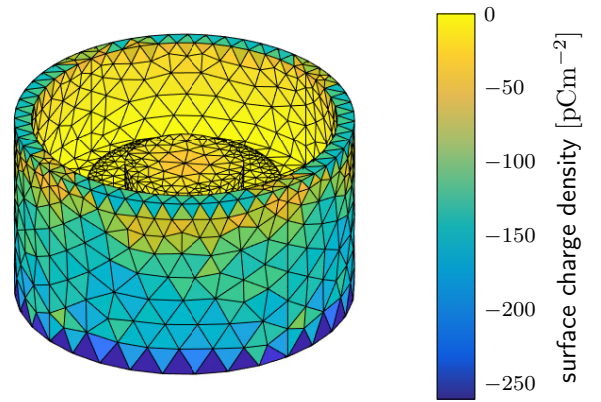


Figure 14: Visualization of the computed surface charge density distribution obtained from the standard PEEC method.

5 Conclusions

This paper proposes a Partial Element Equivalent Circuit (PEEC) method based on the function spaces from Iso-geometric Analysis (IgA). It is applied to electrostatics. Thanks to the use of an integral equation formulation, the adoption of spline-based geometry concepts from IgA and piece-wise constant basis functions, it is shown how a fully-coupled capacitance circuit can be extracted bypassing the usual costly meshing step. This saves time and manual efforts of a potential user. It is demonstrated that a realistic problem with curved geometry can be solved with adequate accuracy. Moreover, the proposed IgA-PEEC method converges for curved geometries up to three times faster than a conventional PEEC implementation.

References

- [1] S. Chakravorti and H. Steinbigler, “Capacitive-resistive field calculation on HV bushings using the boundary-element method,” *IEEE Transactions on Dielectrics and Electrical Insulation*, vol. 5, no. 2, pp. 237–244, 1998.

- [2] S. Monga, R. S. Gorur, P. Hansen, and W. Massey, "Design optimization of high voltage bushing using electric field computations," *IEEE Transactions on Dielectrics and Electrical Insulation*, vol. 13, no. 6, pp. 1217–1224, 2006.
- [3] P. T. Boggs, A. Althsuler, A. R. Larzelere, E. J. Walsh, R. L. Clay, and M. F. Hardwick, "DART system analysis," Sandia National Laboratories, Technical Report, Aug. 2005.
- [4] J. A. Cottrell, T. J. R. Hughes, and Y. Bazilevs, *Isogeometric Analysis: Toward Integration of CAD and FEA*. Wiley, 2009.
- [5] E. Cohen, R. F. Riesenfeld, and G. Elber, *Geometric Modeling with Splines: An Introduction*. CRC Press, 2001.
- [6] A. E. Ruehli, "Equivalent circuit models for three-dimensional multiconductor systems," *IEEE Trans. Microw. Theor. Tech.*, vol. 22, no. 3, pp. 216–221, 1974.
- [7] F. Denz, "Modeling and simulation of varistor-related problems," Dissertation, Technische Universität Darmstadt, Apr. 2014.
- [8] A. E. Ruehli, G. Antonini, and L. Jiang, *The Partial Element Equivalent Circuit Method for Electro-Magnetic and Circuit Problems*, 1st ed. John Wiley & Sons, 2017.
- [9] G. Antonini, A. Ruehli, and J. Esch, "Nonorthogonal PEEC formulation for time and frequency domain modeling," in *2002 IEEE International Symposium on Electromagnetic Compatibility*, vol. 1, 2002, pp. 452–456.
- [10] R. Torchio, "A volume PEEC formulation based on the cell method for electromagnetic problems from low to high frequency," *IEEE Transactions on Antennas and Propagation*, vol. 67, no. 12, pp. 7452–7465, 2019.
- [11] M. Spasojevic and P. Levin, "On adaptive refinement for boundary integral methods in electrostatics," *IEEE Transactions on Dielectrics and Electrical Insulation*, vol. 1, no. 6, pp. 963–974, 1994.
- [12] J. Dölz, H. Harbrecht, S. Kurz, S. Schöps, and F. Wolf, "A fast isogeometric BEM for the three dimensional Laplace- and Helmholtz problems," *Comput. Meth. Appl. Mech. Eng.*, vol. 330, pp. 83–101, 2018.
- [13] J. Dölz, H. Harbrecht, S. Kurz, M. Multerer, S. Schöps, and F. Wolf, "Bembel: The fast isogeometric boundary element C++ library for Laplace, Helmholtz, and electric wave equation," *Software X*, vol. 11, p. 100476, Apr. 2020.
- [14] S. A. Sauter and C. Schwab, *Boundary Element Methods*. Springer. Berlin, Heidelberg, 2011.
- [15] A. Buffa, G. Sangalli, and R. Vázquez, "Isogeometric analysis in electromagnetics: B-splines approximation," *Comput. Meth. Appl. Mech. Eng.*, vol. 199, pp. 1143–1152, 2010.
- [16] A. Buffa, J. Dölz, S. Kurz, S. Schöps, R. Vázquez, and F. Wolf, "Multipatch approximation of the de Rham sequence and its traces in isogeometric analysis," *Numer. Math.*, vol. 144, no. 1, pp. 201–236, Jun. 2019.
- [17] M. G. Duffy, "Quadrature over a pyramid or cube of integrands with a singularity at a vertex," *SIAM J. Numer. Anal.*, vol. 19, no. 6, pp. 1260–1262, 1982.
- [18] F. Freschi, "Fast block-solution of PEEC equations," *IEEE Transactions on Magnetics*, vol. 49, no. 5, pp. 1753–1756, 2013.
- [19] C. Wollenberg and A. Gurisch, "Analysis of 3-d interconnect structures with PEEC using SPICE," *IEEE Transactions on Electromagnetic Compatibility*, vol. 41, no. 4, pp. 412–417, 1999.
- [20] S. Safavi and J. Ekman, "Feasibility analysis of specialized PEEC solvers in comparison to SPICE-like solvers," *Journal of Computational Electronics*, vol. 11, no. 4, pp. 440–452, Dec 2012.
- [21] J. Benoît and G. Guennebaud, "Eigen3 C++ linear algebra template library," official website, eigen.tuxfamily.org. Date of access July 14, 2022.
- [22] OpenMP Architecture Review Board, "OpenMP application program interface version 3.0," May 2008.
- [23] D. J. Jackson, "Boundary representation modelling with local tolerances," in *Proceedings of the Symposium on Solid Modeling and Applications*. ACM, 1995, pp. 247–254.
- [24] M. Nolte, R. Torchio, and S. Schöps, Source code at <http://www.bembel.eu>, doi:10.5281/zenodo.2671596.
- [25] Y. Späck-Leigsnering, E. Gjonaj, and H. de Gersem, "Electrothermal optimization of field grading systems of station class surge arresters," *IEEE Journal on Multiscale and Multiphysics Computational Techniques*, vol. 4, pp. 29–36, 2019.
- [26] M. Gießel, "Elektrothermisches Verhalten von Hochspannungs-Metalloxid-Ableitern mit reduzierten Steuersystemen in Wechselspannungsnetzen," Dissertation, Technische Universität Darmstadt, 2018.